Constant real-space fractal dimensionality and structure evolution in $Ti_{62}Cu_{38}$ metallic glass under high pressure

Liangliang Li,[1,2] Luhong Wang,[1,*] Renfeng Li,[1,2] Haiyan Zhao,[3,4] Dongdong Qu,[5] Karena W. Chapman,[4] Peter J. Chupas,[4] and Haozhe Liu[1,2,†]

[1]*Harbin Institute of Technology, Harbin 150080, China*

[2]*Center for High Pressure Science and Technology Advanced Research, Changchun 130015, China*

[3]*Center for Advanced Energy Studies, University of Idaho, Idaho Falls, Idaho 83406, USA*

[4]*Advanced Photon Source, Argonne National Laboratory, Argonne, Illinois 60439, USA*

[5]*School of Mechanical and Mining Engineering, The University of Queensland, Brisbane, Queensland 4072, Australia*

(Received 11 August 2016; revised manuscript received 21 October 2016; published 7 November 2016)

The structure of binary $Ti_{62}Cu_{38}$ metallic glass is investigated under pressures up to 33.8 GPa using the pair distribution function analysis based on high-energy x-ray scattering and reverse Monte Carlo (RMC) simulations. At a global scale, its relative volume shows a continuously smooth curve as a function of pressure. The isothermal bulk modulus of $Ti_{62}Cu_{38}$ metallic glass is estimated as $B_0 = 132(3)$ GPa with $B_0' = 5.8(0.4)$. At a local scale, the atomic packing structure under compression conditions, which is extracted from RMC simulations, shows that the topological short-range order is dominated by the deformed icosahedron polyhedra and basically maintains stable. From the relationship between the relative volume and changing ratio of the atomic separation distances, the real-space fractal dimensionality of this metallic glass is determined as about 2.5 for all of the first four peaks. This experimental result reveals the consistent nature of the fractal feature on the degree of self-similarity in this sample within the entire experimental pressure range.

DOI: 10.1103/PhysRevB.94.184201

The fractal feature has been suggested in glass systems for many years. Very recently, links between the structures of metallic glasses and fractal dimensionality under high-pressure conditions were discovered [1–3]. A power-law exponent of 2.5 in the relationship between density and the so-called the first strong diffraction peak in reciprocal space was proposed as a universal feature for metallic glasses under compression [2,3]. Furthermore, the fractal dimensionality of metallic glasses in real space was found to remain about 2.5 as well, which was calculated from the atomic nearest-neighbor distance for the pair distribution function (PDF) in two typical binary metallic glasses of Cu-Zr and Ni-Al systems up to 20 GPa from classical molecular dynamics (MD) simulations [1]. More interestingly, the pressure dependence of the crossover feature on the power-law exponent shifting from 2.5 to 3 with increasing atomic separation distance was proposed, which related to the pressure tuning the correlation length change based on the continuum percolation model [1]. However, no experimental PDF data were reported to examine the real-space fractal dimensionality for any metallic glass system and the validity of these fractal features in real space for metallic glass under high-pressure conditions needs to be checked by measured data in addition to the MD simulations. Based on this motivation, a typical binary metallic glass Ti-Cu system, which has been studied at ambient conditions for many years [4–6], was selected as the model for the study of structure and real-space fractal dimensionality under pressure conditions in this paper.

Due to the complexity of the experimental and analytical procedures, investigation of the atomic level structure in real space for nonperiodic systems under high-pressure conditions is exceedingly rare. For example, the limited range of Q in previous high-pressure x-ray-scattering measurements restricted the accuracy of Fourier transforms to real-space PDFs, therefore MD simulations instead of measured PDFs were used to study the structure evolution of metallic glass upon compression [1]. The PDF method is able to provide valuable insights into the local atomic structure and recently became an advanced structure analysis technique combined with the synchrotron high-energy x-ray-scattering measurement in the high-Q range [7,8]. Since the PDF method provides real-space structural information in one dimension, simulations of the total scattering data using modeling techniques, such as reverse Monte Carlo (RMC) simulations, are extremely useful for visualizing the three-dimensional atomic arrangement of liquid and amorphous materials [9,10]. Furthermore, combining the density information derived from the RMC fitting with the measured PDF, the fractal dimensionality of the system, if it exists, can be determined in real space.

The total x-ray-scattering data for metallic glass $Ti_{62}Cu_{38}$ under high pressure at room temperature were collected at the sector 11-ID-B beamline at the Advanced Photon Source, Argonne National Laboratory, using an incident beam with a size of $150 \times 150\,\mu m^2$ and a high energy of 86.7 keV. A two-dimensional large amorphous-silicon-based flat-panel detector was used to record the scattering x ray. A sample with a dimension of $150 \times 150 \times 20\,\mu m^3$ was located in the sample chamber, which is a T301 stainless steel gasket with a 270-μm-diam hole between the two anvils of the diamond anvil cell. The pressure medium was 1:4 methanol/ethanol and pressure was measured using ruby fluorescence method [11].

Raw two-dimensional image data were processed using the FIT-2D [12] software with a masking strategy [13] to mask the diamond peaks to obtain one-dimensional scattering data. After subtracting the contributions from the sample environment and background, the structure factor $S(Q)$ and reduced

*luhong1@hit.edu.cn

†haozhe.liu@hpstar.ac.cn

PDF $G(r)$ were extracted using the PDFGETX2 program [14], which performs a numerical Fourier transformation between $S(Q)$ and $G(r)$ according to

$$G(r) = 4\pi r \rho_0 [g(r) - 1] = \frac{2}{\pi} \int_0^\infty Q[S(Q) - 1] \sin(Qr) dQ, \quad (1)$$

where ρ_0 is the average atomic number density and $g(r)$ is the pair distribution function.

The RMC method was performed using a cubic box with periodic boundary conditions containing 10 000 atoms to fit the x-ray-scattering data for the $Ti_{62}Cu_{38}$ metallic glass using RMC++ [15]. A random initial configuration with a number density of 0.0656 $Å^{-3}$ was used for the ambient pressure RMC fitting, where the density was based on a value measured by the Archimedes method. At high pressure, the number densities were determined by adjusting the simulation box to provide the best match between the RMC and experimental data.

Changes in the structure factor $S(Q)$ and the corresponding PDF for $Ti_{62}Cu_{38}$ metallic glass at various pressure conditions are displayed in Fig. 1. The splitting of the second peak in both $S(Q)$ and the PDF observed at each measured pressure is the characteristic indicator for conventional amorphous systems [16,17]. In reciprocal space, the relation between the first peak position Q_1 and the second peak position Q_2, as well as $Q_{2\text{shoulder}}$, which is the position of the shoulder of the second peak, was proposed to relate to specific types of short-range order [18]. For example, the perfect icosahedron short-range order characterized by Q_2/Q_1 is 1.71 and by $Q_{2\text{shoulder}}/Q_1$ is 2.04 [19] and the short-range order in liquid pure Ti characterized by Q_2/Q_1 is 1.76(0.01) and by $Q_{2\text{shoulder}}/Q_1$ is 1.92(0.01) [20]. Two Gaussian functions are used to fit the second peak and the results show that the ratio of the peak positions Q_2/Q_1 remains about 1.69(0.01) and $Q_{2\text{shoulder}}/Q_1$ about 1.95(0.01), indicating the continuing existence of somewhat distorted icosahedral short-range order in this $Ti_{62}Cu_{38}$ metallic glass [19,20].

With increasing pressure, the first peak position Q_1 of the structure factor $S(Q)$ in reciprocal space shifts towards higher Q, while the nearest-neighbor distance r_1 in real space shifts to shorter distances. These characteristic peak shifts reflect the volume shrinkage and the density increase caused by high pressure. In this work, the density information is derived from RMC simulations. The RMC fit quality at various pressures is also presented in Fig. 1, which displays a good match between the fitting and experimental data. The fitting error of the derived density at each pressure point is within 2.7%. The relative volume V/V_0 of the binary metallic glass $Ti_{62}Cu_{38}$ as a function of pressure is presented in Fig. 2. A decline in volume of about 15% is observed from ambient conditions to 33.8 GPa. Fitting the data by using the third-order Birch-Murnaghan equation of state (EOS), it is shown that the isothermal bulk modulus of $Ti_{62}Cu_{38}$ is $B_0 = 132(3)$ GPa when $B_0' = 5.8(0.4)$. Changes in the relative volume as a function of pressure exhibit a continuously smooth curve, indicating that no detectable phase transition exists within the pressure range investigated in this work.

The first peak position Q_1 and the nearest-neighbor distance r_1 as a function of pressure are shown in insets (a) and (b) of

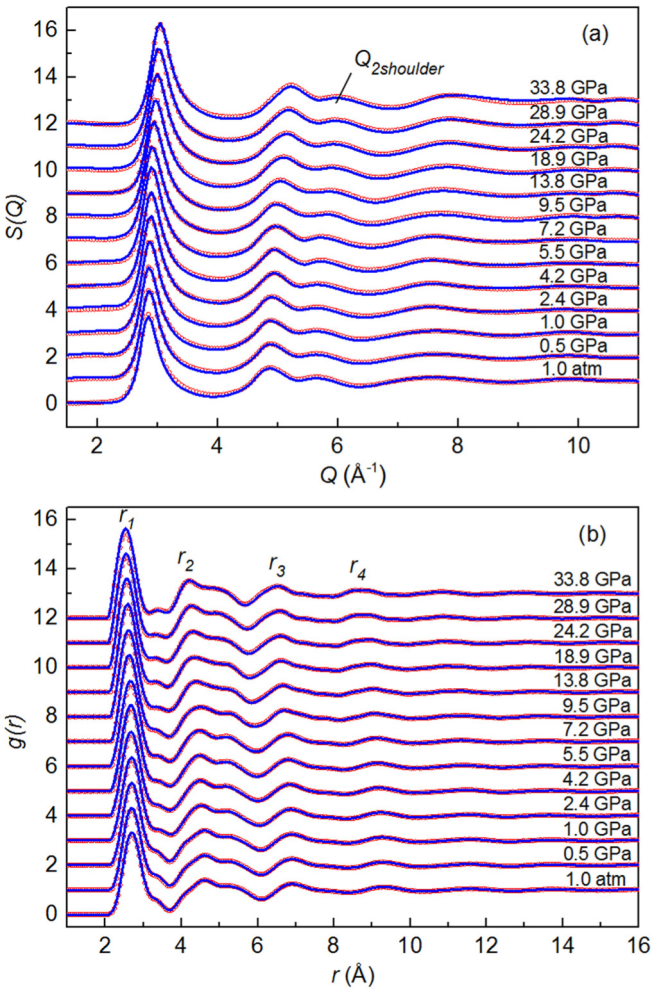

FIG. 1. (a) Experimental structure factor $S(Q)$ and (b) pair distribution function $g(r)$ of the $Ti_{62}Cu_{38}$ metallic glass (blue solid line) at various pressure conditions, with the corresponding RMC fits (red open-circle line).

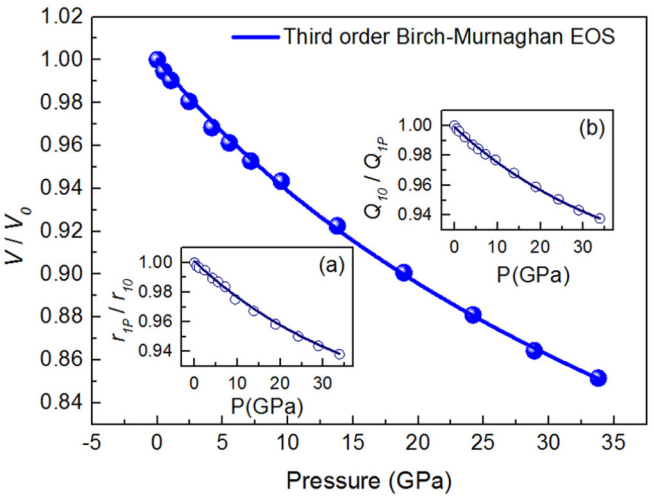

FIG. 2. Relative volume V/V_0 of the $Ti_{62}Cu_{38}$ metallic glass as a function of pressure derived from the RMC fit. The blue solid line shows the data fitting using the third-order Birch-Murnaghan EOS. Inset (a) shows changes in the ratio of the first peak position Q_1 and inset (b) the nearest-neighbor distance r_1 induced by pressure.

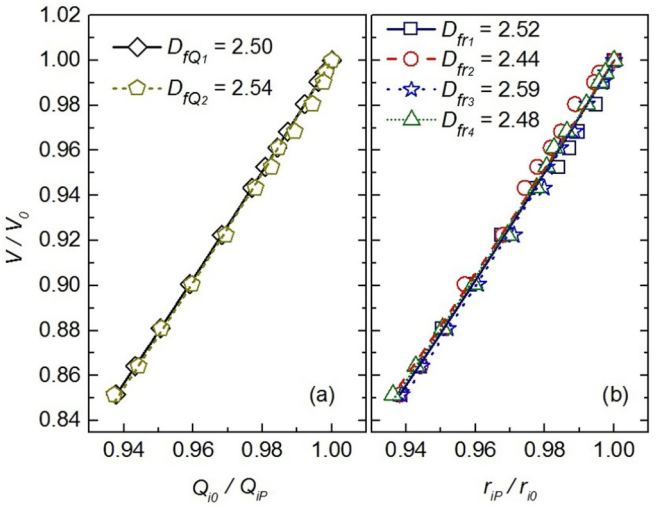

FIG. 3. Relative volume V/V_0 as a function of (a) the ratio of the first and second peak positions in reciprocal space and (b) the ratio of peak position r_i in real space, where $i = 1,2,3$, and 4.

Fig. 2, respectively. The changes in the density related to the first strong peak shifts in both reciprocal space and real space were discovered to follow the power law [1–3]

$$\frac{V}{V_0} = \left(\frac{Q_{10}}{Q_{1p}}\right)^{D_{fQ}} \quad \text{or} \quad \frac{V}{V_0} = \left(\frac{r_{1p}}{r_{10}}\right)^{D_{fr}}, \tag{2}$$

where V_0 is the average atomic volume, Q_{10} is the first peak position of structure factor $S(Q)$, and r_{10} is the nearest-neighbor distance under ambient pressure conditions; V, Q_{1p}, and r_{1p} are the corresponding values under high-pressure conditions; and D_{fQ} and D_{fr} are the power exponents determined by the changing ratio of Q_1 and r_1, respectively. According to the exponent fitting of the power law in formula (2), D_{fQ_1} of 2.50(0.01) is determined in reciprocal space by using value change of Q_1. In real space, D_{fr1} is determined as 2.52(0.04) according to a change in nearest-neighbor distance r_1, as shown in Figs. 3(a) and 3(b), respectively. These results are close to the previous reported values of $D_{fQ1} = 2.50$ [1,2] and $D_{fr1} = 2.54$ in other metallic glass systems from MD simulations [1]. The nonintegers D_{fQ} and D_{fr} reveal these fractal dimensionalities as scale parameters, which reflect the degree of self-similarity in medium-range and short-range ordering in the currently studied metallic glass system, and are in agreement with previous reports [1,2].

From real-space PDF curves at various pressure conditions, fractal dimensionalities were determined by normalized positions of the second peak r_2, the third peak r_3, and the fourth peak r_4 as 2.44(0.05), 2.59(0.02), and 2.48(0.02), respectively, as shown in Fig. 3(b). A roughly consistent fractal dimensionality of about 2.5 is observed, which surprisingly extends far beyond the nearest-neighbor range in real space in this metallic glass system. This is different from the results of previous MD simulations, which suggested that the power-law exponent crossover phenomenon could be common in metallic glass systems [1]. It is well known that the limitation of classical MD simulations strongly depends on the quality of the potential. As pointed out in the Supplemental Material in Ref. [1], the embedded-atomic-method-type potentials used in its MD simulations normally are not tested for high-pressure conditions, which may result in errors. Thus the simulated crossover of the power-law exponent from about 2.5 to 3 with increasing atomic separation distance in real space might not be a general feature in metallic glass systems, at least not for this Ti-Cu glass system. Instead, from the current measured PDF data, the real-space fractal dimensionality could remain constant about 2.5 over a large pair distribution range up to above 30-GPa conditions. This consistent nature of fractal dimensionality from various PDF peaks in real space reflects the constant degree of self-similarity in various building block domains in this system, which actually works well in a much bigger atomic separation distance range than that in previous MD simulations [1]. This discovery improves the understanding for the real-space fractal feature in metallic glass and offers a practical way for the challenging density estimation for nonperiodic systems under high-pressure conditions by using their measured PDF regardless of the crossover in its power-law exponent when the pressure is close to 15–20 GPa [1].

For the PDF peaks higher than the fourth one, the relations between V_p/V_0 and r_{ip}/r_{i0} ($i > 4$) become featureless and could not be fitted according to Eq. (2). This might be related to the limitation effect of the correlation length and needs more measured data to prove its generality in metallic glass systems. The asymptotic behavior of these PDFs in the higher-r range could be related to the fractal feature, which was proposed by Ma *et al.* [21]. A sinusoidal function was introduced to describe the oscillatory correlation at the far end of the PDF curves in real space, following the early fractal model on the colloidal system [22]

$$g(r) = (A/r^{D-D_f})\exp(-r/\xi)\sin(Q_1 r - \phi) + 1, \tag{3}$$

where A is the amplitude, $D = 3$ is the dimensionality in three-dimensional Euclidean space, ξ is the cutoff length, Q_1 is the position of the first strong diffraction peak in reciprocal space, and ϕ is a phase. In the $Ti_{68}Cu_{32}$ metallic glass system, $D_f = 2.51$ applied in this equation is the average of D_{fi}, where $i = 1,2,3,4$.

However, this fractal model of asymptotic behavior was challenged by a recent study based on binary alloy liquid cases [23], in which the asymptotic behavior of their PDFs could also be fitted well by the Ornstein-Zernike (OZ) model, which is a pole analysis for binary systems [24,25]. In the OZ approach, asymptotic behavior of the PDF could be described as

$$g(r) = (2|\mathcal{A}|/r)\exp(-r/\varepsilon)\sin(Q_1 r - \theta) + 1, \tag{4}$$

where $\mathcal{A}$ is the amplitude, θ is a phase, and ε is the decay length. As pointed out previously [23], the only significant difference between Eqs. (3) and (4) is the power exponent of r.

Using Eqs. (3) and (4), three sets of typical $g(r)$ curves under various pressure conditions were selected for the fitting as shown in Fig. 4. It is clear that both equations mathematically fit almost equally well for the high-r range from the fourth peak to 29.99 Å, as indexed by the very close values for the goodness-of-fit parameters R^2. All the fitting parameters are summarized in Table I. The fitting results present a tradeoff effect, i.e., the bigger D_f is, the smaller the cutoff or decay length would be. It is noted that physical models corresponding to two equations are quite different, as discussed previously [23]. Therefore, good fitting of both

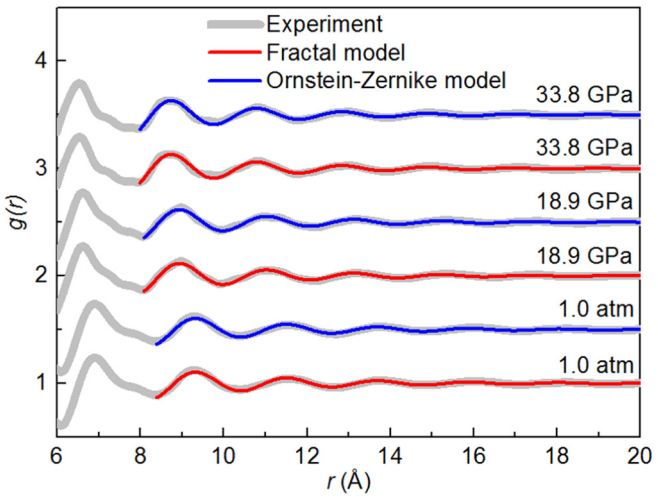

FIG. 4. Fitting results of the asymptotic decay in the large-r range for three sets of typical $g(r)$ using the fractal and OZ approaches. The thick gray line represents the $g(r)$ from experiment. The thin red and blue lines show fits of the fractal and OZ models, respectively.

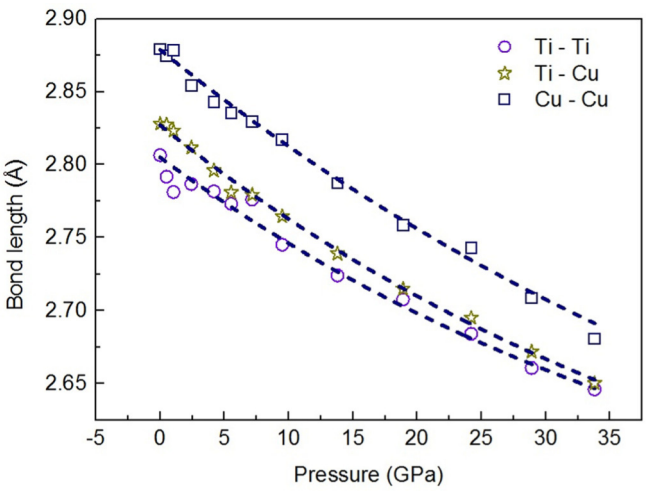

FIG. 5. Bond distance as a function of the pressure. The Cu-Cu, Ti-Ti, and Ti-Cu bond lengths are represented by open circles, open squares, and open stars, respectively.

equations suggests that the proposed asymptotic decay fitting [21] is not the practice method to obtain physically reliable parameters for fractal dimensionality. Instead, the method of relative change of the individual peak position in the real-space PDF could provide more stable scale invariance for fractal dimensionality.

It is interesting to compare the fractal feature between the $Ti_{68}Cu_{32}$ metallic glass system under high pressure with other available high-pressure cases, such as the metallic system of liquid gallium. The fractal dimensionality in the $Ti_{68}Cu_{32}$ metallic glass system is determined to be uniformly about 2.5 from the first four PDF peaks. In contrast, in liquid gallium, the power exponent D_f extracted from both the third and fourth peaks is smaller than 3, whereas from both the first and second peaks it is bigger than 3, estimated from the measured data [26]. The corresponding parameters of fractal dimensionality in liquid Ga depend on the PDF peak positions, which demonstrate unique physical features and indicate a more complicated feature than metallic glass cases.

Information on the atomic packing characteristics, such as the bond length, atomic coordination number, and local atomic environment, can be extracted from the RMC atomic configurations using the Voronoi tessellation technique [27,28]. The Voronoi polyhedra are indexed by $\langle n_3,n_4,n_5,n_6,\ldots\rangle$ to specify the polyhedron type and describe the local environment of the associated central atom, where n_i denotes the number of i-edged faces of a Voronoi polyhedron.

The bond length derived from the Voronoi polyhedron provides information on the interatomic distance's shortening trend as the pressure increases, as shown in Fig. 5. In particular, the bond length ratio between the solute and solvent atoms, referred to as the effective atomic size ratio, controls the coordination number (CN) [29,30]. The effective atomic size ratio in the metallic glass $Ti_{62}Cu_{38}$ studied herein is 1.02 and this ratio remains nearly constant with increasing pressure. The stable effective atomic size ratio generally leads to the dominant CNs within the first nearest-neighbor shell, which are dominated by CNs of 12, 13, and 14 as shown in Fig. 6(a), not changing with increasing pressure. By the same token, the average CN, Ti-centered average CN, and Cu-centered average CN in this metallic glass $Ti_{62}Cu_{38}$ are nearly constant at 13.06(0.04), 12.86(0.06), and 13.39(0.07), respectively, in the first nearest-neighbor shell. This modeling result is similar to the result of other metallic glass, such as the $Pd_{81}Si_{19}$ system upon compression above 30 GPa, where the CN remains unchanged with increasing pressure as well [31]. Additionally, it is also found that the CN determined by the effective atomic size ratio causes the Cu-centered average CN to be greater than the Ti-centered CN [30].

The effective atomic size ratio is also correlated with the type of coordination polyhedra under pressure [30]. The nearly unchanged effective atomic size ratio leads to the frequencies of the dominant coordination polyhedral types being similar and only slightly fluctuating with increasing pressure. The frequencies of the dominant Voronoi polyhedra within the first

TABLE I. Parameters obtained by fitting three sets of selected $g(r)$ to Eq. (3) based on the fractal model and to Eq. (4) based on the OZ model.

		Fractal model				OZ model			
Pressure	Range (Å)	R^2	ξ (Å)	A	ϕ	R^2	ε (Å)	$\mathcal{A}$	θ
1.0 atm	8.39–29.99	0.958	3.47(8)	4.6(3)	0.27(1)	0.958	4.14(9)	4.6(3)	0.27(1)
18.9 GPa	8.09–29.99	0.969	3.25(6)	5.4(3)	0.26(1)	0.969	3.85(8)	5.3(3)	0.26(1)
33.8 GPa	7.99–29.99	0.957	3.06(7)	6.7(5)	0.26(1)	0.958	3.60(9)	6.6(5)	0.26(1)

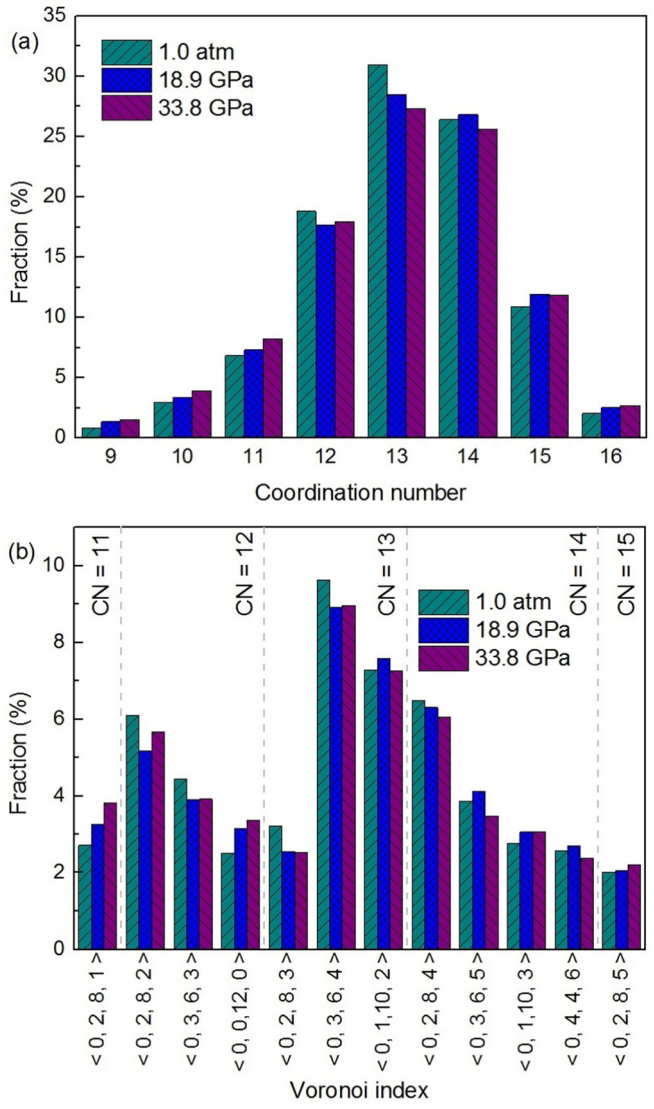

FIG. 6. (a) The CN distributions and (b) fractions of dominant coordination polyhedra in $Ti_{62}Cu_{38}$ metallic glass under selected pressure conditions of 1.0 atm, 18.9 GPa, and 33.8 GPa. Similar trends are found at other pressure points. Note that only the polyhedra with a fraction more than 2% are shown.

nearest-neighbor shell under three representative pressures of 1.0 atm, 18.9 GPa, and 33.8 GPa are illustrated in Fig. 6(b). Note that there is a one-to-one correspondence between the Voronoi index and the coordination polyhedron. Voronoi polyhedra with indices $\langle 0,2,8,1\rangle$ and $\langle 0,0,12,0\rangle$ corresponding to the deformed prism and icosahedron polyhedra, respectively, both contribute to a small fraction in this system. The polyhedra of the deformed crystal feature, which are indexed by $\langle 0,3,6,4\rangle$, $\langle 0,3,6,5\rangle$, $\langle 0,4,4,6\rangle$, and $\langle 0,2,8,5\rangle$, contribute 18.1% and 17.0% to the entire system, at 1.0 atm and 33.8 GPa, respectively. In contrast, at 1.0 atm and 33.8 GPa, the deformed icosahedron polyhedra indexed by $\langle 0,2,8,2\rangle$, $\langle 0,3,6,3\rangle$, $\langle 0,1,10,2\rangle$, $\langle 0,2,8,3\rangle$, $\langle 0,2,8,4\rangle$, $\langle 0,1,10,3\rangle$, and $\langle 0,1,10,4\rangle$ amount to large fractions of 30.3% and 28.5%, respectively. This clearly indicates that the deformed icosahedron is the main topological short-range order in the $Ti_{62}Cu_{38}$ metallic glass, which is consistent with the results obtained from the Q_2/Q_1 and $Q_{2\text{shoulder}}/Q_1$ ratios analyses. At the local scale, the structure of the $Ti_{62}Cu_{38}$ metallic glass is basically stable as a function of pressure.

In summary, $Ti_{62}Cu_{38}$ metallic glass was investigated using *in situ* synchrotron high-energy x-ray scattering combined with the PDF analysis and RMC fitting under high pressure. The relative volume as a function of pressure was determined as a continuously smooth curve. No major changes existed in the effective atomic size ratio, CN, and dominant polyhedron type at various pressure conditions, which indicated the absence of pressure-induced polyamorphism. Moreover, the real-space fractal dimensionality as an index of the degree of self-similarity in this system remained constant at about 2.5, revealing its intrinsic fractal nature within a large atomic separation distance up to about 10.5 Å in the entire pressure region up to 33.8 GPa.

This work was performed at Argonne National Laboratory and use of the Advanced Photon Source was supported by the U.S. Department of Energy, Office of Science, Office of Basic Energy Sciences, under Contract No. DE-AC02-06CH11357. This work was partially supported by Natural Science Foundation of China (Grants No. U1530402 and No. 11374075), Heilongjiang Province Science Fund for Distinguished Young Scholars (Grant No. JC201005), Heilongjiang Natural Science Foundation (Grant No. E200948), Longjiang Scholar, the Fundamental Research Funds for the Central Universities (Grants No. HIT.BRET1.2010002 and No. HIT.IBRSEM.A.201403), HIT-Argonne Overseas Collaborative Base Project, and Chinese Scholarship Council.

[1] D. Z. Chen, C. Y. Shi, Q. An, Q. Zeng, W. L. Mao, W. A. Goddard, and J. R. Greer, Science **349**, 1306 (2015).
[2] Q. Zeng, Y. Lin, Y. Liu, Z. Zeng, C. Y. Shi, B. Zhang, H. Lou, S. V. Sinogeikin, Y. Kono, C. Kenney-Benson, C. Park, W. Yang, W. Wang, H. Sheng, H.-k. Mao, and W. L. Mao, Proc. Natl. Acad. Sci. **113**, 1714 (2016).
[3] Q. Zeng, Y. Kono, Y. Lin, Z. Zeng, J. Wang, S. V. Sinogeikin, C. Park, Y. Meng, W. Yang, H.-K. Mao, and W. L. Mao, Phys. Rev. Lett. **112**, 185502 (2014).
[4] K. H. J. Buschow, Acta Metal. **31**, 155 (1983).
[5] K. B. Kim, K. A. Song, X. F. Zhang, and S. Yi, Appl. Phys. Lett. **92**, 241915 (2008).
[6] J. J. Pang, M. J. Tan, and K. M. Liew, Appl. Phys. A **106**, 597 (2012).
[7] K. A. See, K. W. Chapman, L. Zhu, K. M. Wiaderek, O. J. Borkiewicz, C. J. Barile, P. J. Chupas, and A. A. Gewirth, J. Am. Chem. Soc. **138**, 328 (2016).
[8] P. J. Chupas, K. W. Chapman, and P. L. Lee, J. Appl. Cryst. **40**, 463 (2007).
[9] R. L. McGreevy and L. Pusztai, Mol. Simul. **1**, 359 (1988).

[10] R. L. McGreevy, J. Phys. Condens. Matter **13**, R877 (2001).
[11] H. K. Mao, J. Xu, and P. M. Bell, J. Geophys. Res. **91**, 4673 (1986).
[12] A. P. Hammersley, J. Appl. Cryst. **49**, 646 (2016).
[13] K. W. Chapman, P. J. Chupas, G. J. Halder, J. A. Hriljac, C. Kurtz, B. K. Greve, C. J. Ruschman, and A. P. Wilkinson, J. Appl. Cryst. **43**, 297 (2010).
[14] X. Qiu, J. W. Thompson, and S. J. L. Billinge, J. Appl. Cryst. **37**, 678 (2004).
[15] O. Gereben, P. Jóvári, L. Temleitner, and L. Pusztai, J. Optoelectron. Adv. Mater. **9**, 3021 (2007).
[16] H. R. Wendt and F. F. Abraham, Phys. Rev. Lett. **41**, 1244 (1978).
[17] R. S. Liu, D. W. Qi, and S. Wang, Phys. Rev. B **45**, 451 (1992).
[18] H. W. Sheng, E. Ma, H. Z. Liu, and J. Wen, Appl. Phys. Lett. **88**, 171906 (2006).
[19] K. F. Kelton, G. W. Lee, A. K. Gangopadhyay, R. W. Hyers, T. J. Rathz, J. R. Rogers, M. B. Robinson, and D. S. Robinson, Phys. Rev. Lett. **90**, 195504 (2003).
[20] G. W. Lee, A. K. Gangopadhyay, K. F. Kelton, R. W. Hyers, T. J. Rathz, J. R. Rogers, and D. S. Robinson, Phys. Rev. Lett. **93**, 037802 (2004).
[21] D. Ma, A. D. Stoica, and X. L.Wang, Nat. Mater. **8**, 30 (2009).
[22] T. Freltoft, J. K. Kjems, and S. K. Sinha, Phys. Rev. B **33**, 269 (1986).
[23] P. Chirawatkul, A. Zeidler, P. S. Salmon, S. Takeda, Y. Kawakita, T. Usuki, and H. E. Fischer, Phys. Rev. B **83**, 014203 (2011).
[24] R. Evans, R. J. F. Leote de Carvalho, J. R. Henderson, and D. C. Hoyle, J. Chem. Phys. **100**, 591 (1994).
[25] R. J. F. Leote de Carvalho and R. Evans, Mol. Phys. **83**, 619 (1994).
[26] O. F. Yagafarov, Y. Katayama, V. V. Brazhkin, A. G. Lyapin, and H. Saitoh, Phys. Rev. B **86**, 174103 (2012).
[27] J. L. Finney, Proc. R. Soc. London Ser. A **319**, 479 (1970).
[28] J. L. Finney, Nature (London) **266**, 309 (1977).
[29] H. W. Sheng, W. K. Luo, F. M. Alamgir, J. M. Bai, and E. Ma, Nature (London) **439**, 419 (2006).
[30] H. W. Sheng, Y. Q. Cheng, P. L. Lee, S. D. Shastri, and E. Ma, Acta Mater. **56**, 6264 (2008).
[31] H. B. Lou, L. H. Xiong, A. S. Ahmad, A. G. Li, K. Yang, K. Glazyrin, H. P. Liermann, H. Franz, X. D. Wang, Q. P. Cao, D. X. Zhang, and J. Z. Jiang, Acta Mater. **81**, 420 (2014).